

COMPACT BINARY FORMATION IN OPEN STAR CLUSTERS II: DIFFICULTY OF GAIA NS FORMATION IN LOW-MASS STAR CLUSTERS

ATARU TANIKAWA¹, LONG WANG^{2,3}, AND MICHIKO S. FUJII⁴

¹Center for Information Science, Fukui Prefectural University, 4-1-1 Matsuoka Kenjojima, Eiheiji-cho, Fukui 910-1195, Japan

²School of Physics and Astronomy, Sun Yat-sen University, Daxue Road, Zhuhai, 519082, China

³CSST Science Center for the Guangdong-Hong Kong-Macau Greater Bay Area, Zhuhai, 519082, China and

⁴Department of Astronomy, Graduate School of Science, The University of Tokyo, 7-3-1 Hongo, Bunkyo-ku, Tokyo 113-0033, Japan

Version May 17, 2024

ABSTRACT

Gaia mission offers opportunities to search for compact binaries not involved in binary interactions (hereafter inert compact binaries), and results in the discoveries of binaries containing one black hole (BH) or one neutron star (NS), called “Gaia BHs” and “Gaia NSs”, respectively. We have assessed if Gaia BHs and NSs can be formed in open clusters through dynamical interactions. In order to obtain a large number of inert compact binaries similar to Gaia BHs and NSs, we have performed gravitational N -body simulations for a large number of open clusters whose total mass is $1.2 \times 10^8 M_{\odot}$. These clusters have various masses, metallicities, densities, and binary fractions. We have found that open clusters form Gaia BHs (10^{-6} - $10^{-5} M_{\odot}^{-1}$) much more efficiently than Gaia NSs ($\lesssim 10^{-7} M_{\odot}^{-1}$) for any cluster parameters. This is quite inconsistent with observational results, because the reported numbers of Gaia BHs and NSs are 3 and 21, respectively. Additionally, we have switched off NS natal kicks for 10^4 open clusters each weighing $10^3 M_{\odot}$ in order to retain a large number of NSs in open clusters. Then, open clusters form inert NS binaries originating from primordial binaries rather than formed through dynamical interactions. This means that Gaia NSs are formed dominantly on isolated fields, not in open clusters, if there is no NS natal kick. We have concluded that Gaia BHs can be dominantly formed in open clusters, however Gaia NSs cannot.

1. INTRODUCTION

Black holes (BHs) and neutron stars (NSs) are compact objects left behind after the deaths of massive stars. They are clues to physical processes involved in massive star evolution, and experimental sites of strong gravitational fields. Thus, they have been explored vigorously. Because of their darkness, only active BHs and NSs have been discovered until quite recently. Active compact objects can be X-ray binaries (see Casares et al. 2017, for review), gravitational wave sources (Abbott et al. 2019, 2021, 2023), and pulsars (see Philippov & Kramer 2022, for review).

Very recently, inactive compact objects have started to be discovered. Mainly, they are binary members, because they are found through binary motions. They are called “non-interacting”, “detached”, “dormant”, or “inert” compact binaries. Hereafter, we unify the notation with inert compact binaries throughout this paper. Such inert compact binaries have been discovered by spectroscopic observations (Giesers et al. 2018; Shenar et al. 2022), and by astrometric observations (El-Badry et al. 2023b,c; Tanikawa et al. 2023; Chakrabarti et al. 2023) with the help of Gaia DR3 (Gaia Collaboration et al. 2023a,b; see review by El-Badry 2024a). Gaia DR3 seems to contain more inert compact binaries according to several candidate lists (Andrews et al. 2022; Shahaf et al. 2023b,a; Jayasinghe et al. 2023; Rowan et al.

2024). Although other inert compact binaries have been reported (Liu et al. 2019; Thompson et al. 2019; Rivinius et al. 2020; Jayasinghe et al. 2021, 2022; Lennon et al. 2022; Saracino et al. 2022), their discoveries have been called into question (Abdul-Masih et al. 2020; Bodensteiner et al. 2020; El-Badry & Quataert 2020, 2021; van den Heuvel & Tauris 2020; El-Badry & Burdge 2022; El-Badry et al. 2022a,b). In addition to inert compact binaries, several single BHs/NSs have been detected by microlensing observations (Lam et al. 2022; Sahu et al. 2022; Howil et al. 2024).

Gaia BH1 and BH2 (hereafter Gaia BHs), which are inert BH binaries discovered from Gaia DR3, and named by El-Badry et al. (2023b,c), have two impacts. First, Gaia BHs have the longest orbital periods among BH binaries discovered so far. In particular, Gaia BH2 breaks the record of BH binary periods by 10 times. These discoveries give the impression that Gaia’s astrometric observations open up a new parameter space of BH binaries. Second, Gaia BHs are hard to form through isolated binary evolution. If Gaia BHs are formed through isolated binary evolution, common envelope ejection should be 10 times more efficient than expected (Chawla et al. 2022; El-Badry et al. 2023b; Shikauchi et al. 2023; but see Kotko et al. 2024). However, a recent study has not supported such efficient common envelope ejection for stars massive enough to form BHs (Hirai & Mandel 2022). Triple stars (El-Badry et al. 2023b,c; Genozov & Perets 2023) and open clusters (Shikauchi et al.

2020; Rastello et al. 2023; Tanikawa et al. 2024; Di Carlo et al. 2024) have been suggested as formation sites of Gaia BHs. Because Gaia BHs are the Galactic disk components, it is difficult to suppose that they are formed in globular clusters and galactic centers.

During the review process of this paper, Gaia BH3 has been reported by Gaia Collaboration et al. (2024). It could belong to the ED-2 stream, which is possibly a tidally disrupted globular cluster (Balbinot et al. 2024). Thus, it would be formed through dynamical interactions in the globular cluster (Marín Pina et al. 2024), which is similar to Gaia BH formation in open clusters (Shikauchi et al. 2020; Rastello et al. 2023; Tanikawa et al. 2024; Di Carlo et al. 2024). However, Gaia BH3 could be formed from isolated binaries (El-Badry 2024b; Iorio et al. 2024), since it is a very metal-poor binary, $[\text{Fe}/\text{H}] = -2.56$ (Gaia Collaboration et al. 2024). The origin of Gaia BHs is an open question.

El-Badry et al. (2024b) have discovered Gaia NS1 which is most likely to be the first inert NS binary from Gaia DR3 (Gaia Collaboration et al. 2023b). The NS candidate mass ($\sim 1.9M_{\odot}$) is higher than other inert NS binary candidates which could be a massive white dwarfs (WDs) as described in the literature (Geier et al. 2023; Zheng et al. 2023). Gaia NS1 is hard to form through isolated binary evolution without efficient common envelope ejection, similarly to Gaia BHs. El-Badry et al. (2024b) have also mentioned that they have found about 20 more inert NS binaries, called ‘‘Gaia NSs’’ hereafter. El-Badry et al. (2024a) have published their detail information during the review process of this paper. This should imply that Gaia NSs are formed more efficiently than Gaia BHs for the following two reasons. First, the number of Gaia NSs discovered is larger than that of Gaia BHs discovered. Second, Gaia NSs is harder to detect than Gaia BHs, because NSs indicate smaller astrometric signals than BHs; NSs swing around their companions less strongly than BHs due to their smaller masses. Another importance of Gaia NS1 is its eccentricity. The eccentricity is ~ 0.1 (El-Badry et al. 2024b), while Gaia BH1 and BH2 have ~ 0.5 (El-Badry et al. 2023b,c). The eccentricity of Gaia NS1 may be too small to be formed through dynamical interactions. We also look into the eccentricities of all the Gaia NSs.

In this paper, we test if open clusters can form Gaia NSs more efficiently than Gaia BHs by means of gravitational N -body simulations. We have found that the formation rate of Gaia NSs is much smaller than that of Gaia BHs if we adopt the conventional single and binary star models. Open clusters cannot retain enough NSs to form Gaia NSs because of their large natal kicks. In order to retain a sufficiently large number of Gaia NSs in open clusters, we switch off natal kicks of NSs, although this assumption is unrealistic. Nevertheless, the formation rate of Gaia NSs is still comparable to that of Gaia BHs, in contrast to the observational implication.

The structure of this paper is as follows. We describe our simulation method in section 2. We show our results in section 3. We discuss if Gaia NSs can be formed in open clusters in section 4. We summarize this paper in section 5.

2. METHOD

We use an N -body code PETAR (Wang et al. 2020b), which is based on the particle-tree and particle-particle algorithm (Oshino et al. 2011; Iwasawa et al. 2017), and highly parallelized by Framework for Developing Particle Simulator with Message Passing Interface, OpenMP, and Single Instruction Multiple Data (FDPS; Iwasawa et al. 2016, 2020). The slow-down algorithmic regularization method (SDAR; Wang et al. 2020a) treats binary orbits and close encounters in order to keep high accuracy efficiently. The Galactic potential is modeled by GALPY (Bovy 2015). Single and binary star evolutions are implemented with the BSE code (Hurley et al. 2000, 2002; Banerjee et al. 2020). Common envelope evolution is the most important process to form compact binaries. The BSE code deals with common envelope evolution, adopting the α formalism (Webbink 1984). We adopt $\alpha_{\text{CE}} = 1$ and λ_{CE} of Claeys et al. (2014). The choice of α_{CE} prevents inert compact binaries from being formed from primordial binaries.

NS population retained in open clusters largely depends on NS natal kicks. Here, we remark on NS natal kicks in our model. NSs receive kick velocities at their births because of asymmetric supernova explosions. The kick velocities are quite different between NSs born from electron capture (EC) and core collapse (CC) supernovae (SNe). In our model, a star causes a CCSN when its carbon-oxygen (CO) core exceeds both of the Chandrasekhar mass limit ($1.44M_{\odot}$ here) and $0.773M_{\text{c,he}} - 0.35M_{\odot}$, where $M_{\text{c,he}}$ is the He core mass of the star. NSs left behind CCSNe have kick velocity distribution given by a single Maxwellian with $\sigma_{\text{k,ccsn}} = 265 \text{ km s}^{-1}$ (Hobbs et al. 2005). If the NSs acquires on fallback mass, the kick velocities are reduced by $1 - f_{\text{fallback}}$, where f_{fallback} is the fraction of the fallback mass (Fryer et al. 2012). This prescription is also applied to BH natal kicks. ECSNe (Miyaji et al. 1980; Nomoto 1984, 1987; van den Heuvel 2007) are thought to raise much smaller kick velocities than CCSNe because of slightly asymmetric explosion (Jones et al. 2013; Gessner & Janka 2018). In our model, a star generates an ECSN when it does not cause a CCSN, and its CO core mass is $\geq 1.6M_{\odot}$. Their natal kick velocities are expressed by a single Maxwellian with 3 km s^{-1} (Podsiadlowski et al. 2004; Gessner & Janka 2018). About 1 % of NSs are formed from ECSNe under the initial mass function we adopt.

NSs with small natal kicks can be formed from accreting WDs (Baron et al. 1987; Nomoto & Kondo 1991; Woosley & Baron 1992; Fryer et al. 1999; Dessart et al. 2006; Abdikamalov et al. 2010; Mori et al. 2023; Longo Micchi et al. 2023). This channel is called accretion-induced collapse (AIC). Such NSs could be inside of globular clusters (Ivanova et al. 2008; Kremer et al. 2023). In our simulations, this channel is achieved from two paths. First, an oxygen-neon (ONe) WD increases its mass to the Chandrasekhar mass limit, accreting materials through mass transfer from its MS or post-MS (PMS) companion (non-degenerate companion). Second, two WDs merge without explosion. We describe the second path, since it is not implemented in previous BSE codes. We suppose that WD mergers create NSs under the following conditions.

1. The total mass of two WDs exceeds the Chandrasekhar mass limit.

2. Neither of two WDs is a HeWD. Such WD merger products are thought to explode due to the double detonation scenario (Nomoto 1982; Woosley et al. 1986) in double WD systems (Perets et al. 2010; Guillochon et al. 2010; Pakmor et al. 2013, 2021; Shen et al. 2018; Tanikawa et al. 2018, 2019; Gronow et al. 2020; Ferrand et al. 2022; Zenati et al. 2023; El-Badry et al. 2023a).
3. Both of two WDs do not consist of two carbon-oxygen (CO) WDs with $\geq 0.8M_{\odot}$. This type of merger products can experience explosion due to the violent merger scenario (Pakmor et al. 2010, 2011, 2012a,b). This condition is referred from Sato et al. (2015, 2016). Note that this criterion naturally includes an explosion due to the spiral instability (Kashyap et al. 2015).

These conditions are motivated by binary population synthesis modeling of type Ia SNe from WD mergers (Toonen et al. 2012; Ruiter 2019). We assume that two WD merger creates a NS with the following properties.

1. No natal kick. AIC develops only small asymmetry, similarly to an ECSN (Dessart et al. 2006; Schwab et al. 2015).
2. The same mass as the total mass of the two WDs. WD mergers trigger nuclear reactions, however eject at most $0.1M_{\odot}$ (Dan et al. 2014; Kashyap et al. 2018). Although the system can eject its mass during AIC, the ejecta mass is at most $\sim 0.01M_{\odot}$ (Dessart et al. 2006; Mori et al. 2023; Longo Micchi et al. 2023). The total mass of a WD merger product ($\gtrsim 1.4M_{\odot}$) is larger than mass loss from the WD merger to AIC ($\sim 0.1M_{\odot}$). Thus, we assume that the system loses no mass from the merger to AIC.

In Table 1, we summarize our cluster models. In the fiducial model, the initial cluster mass (M) and stellar metallicity (Z) are $1000M_{\odot}$ and 0.02, respectively. A cluster is on a circular orbit at the distance of 8 kpc from the Galactic center. The initial cluster mass density ρ is $20M_{\odot} \text{ pc}^{-3}$, where ρ is defined as mass density inside the half-mass radius of a cluster. The initial binary fraction depends on primary star masses (m_1). The initial binary fraction for $m_1 \geq 5M_{\odot}$ ($f_{b,\geq 5M_{\odot}}$) is unity (or 100 %), while the initial binary fraction for $m_1 < 5M_{\odot}$ ($f_{b,< 5M_{\odot}}$) is 0.2. Note that the initial binary fraction is defined as $N_b/(N_s + N_b)$, where N_s and N_b are the numbers of single and binary stars, respectively. Single stars and primary stars in binaries have Kroupa’s initial mass function (Kroupa 2001) in the range from $0.08M_{\odot}$ to $150M_{\odot}$. When the primary star of a binary has more than or equal to $5M_{\odot}$, the binary mass ratio (q), orbital period (P), and orbital eccentricity (e) distributions are subject to initial conditions of Sana et al. (2012): $f(q) \propto q^{-0.1}$ ($0.1 \leq q \leq 1$), $f(\log P) \propto (\log P)^{-0.55}$ ($0.15 < \log(P/\text{day}) < 5.5$), and $f(e) \propto e^{-0.42}$ ($0 \leq e \leq 1$). When the primary star of a binary has less than $5M_{\odot}$, the binary mass ratio (q), orbital period (P), and orbital eccentricity (e) distributions are subject to initial conditions of Kroupa (1995a,b) with modification of Belloni et al. (2017): $f(q) \propto \text{const}$,

TABLE 1
SUMMARY OF MODELS. PARAMETERS INDICATED BY “–” ARE THE SAME AS THOSE OF THE FIDUCIAL MODEL.

Name	M [M_{\odot}]	Z	ρ [$M_{\odot} \text{ pc}^{-3}$]	$f_{b,< 5M_{\odot}}$	$\sigma_{k,\text{ccsn}}$ [kms^{-1}]
Fiducial	1000	0.02	20	0.2	265
$M = 200M_{\odot}$	200	–	–	–	–
$M = 500M_{\odot}$	500	–	–	–	–
$M = 2000M_{\odot}$	2000	–	–	–	–
$Z = 0.01$	–	0.01	–	–	–
$Z = 0.005$	–	0.005	–	–	–
$Z = 0.002$	–	0.002	–	–	–
$Z = 0.0002$	–	0.0002	–	–	–
$\rho = 2$	–	–	2	–	–
$\rho = 200$	–	–	200	–	–
$f_{b,< 5M_{\odot}} = 0$	–	–	–	0	–
$f_{b,< 5M_{\odot}} = 0.5$	–	–	–	0.5	–
No-kick	–	0.002	–	–	0

$f(\log P) \propto (\log(P/\text{day}) - 1)/(45 + [\log(P/\text{day}) - 1]^2)$ ($10 \leq P/\text{day} \leq 10^{8.43}$), and $f(e) \propto e$. We make These initial conditions by means of MCLUSTER (Küpper et al. 2011). The simulations are finished at 1 Gyr.

We prepare cluster models in which one parameter is different from those in the fiducial model. The $M = 200M_{\odot}$, $M = 500M_{\odot}$ and $M = 2000M_{\odot}$ models have clusters with the initial masses of $200M_{\odot}$, $500M_{\odot}$ and $2000M_{\odot}$, respectively. The $Z = 0.01$, $Z = 0.005$, $Z = 0.002$, and $Z = 0.0002$ models have clusters with stellar metallicities of $Z = 0.01$, 0.005, 0.002, and 0.0002 respectively. The $\rho = 2$ and $\rho = 200$ models have clusters with the initial mass densities of 2 and $200M_{\odot} \text{ pc}^{-3}$, respectively. The $f_{b,< 5M_{\odot}} = 0$ and $f_{b,< 5M_{\odot}} = 0.5$ models have $f_{b,< 5M_{\odot}} = 0$ and 0.5, respectively. Note that $f_{b,\geq 5M_{\odot}}$ is fixed to unity, which is reasonable according to Sana et al. (2012) and Moe & Di Stefano (2017).

Additionally, we make the no-kick model in which no CCSNe generate kick velocities, in order to investigate effects of CCSN natal kicks. We set the metallicity to $Z = 0.002$, because the visible star of Gaia NS1 has small metallicity, $[\text{Fe}/\text{H}] = -1.23$ (El-Badry et al. 2024b).

We generate a large number of open clusters with different realizations, so that each model contains 10^7M_{\odot} open clusters in total. The total mass of simulated clusters is $1.3 \times 10^8M_{\odot}$. We can expect that we obtain ~ 100 Gaia BHs from each cluster model, because the formation efficiency of Gaia BHs is $\sim 10^{-6}M_{\odot}^{-1}$ (Rastello et al. 2023; Tanikawa et al. 2024; Di Carlo et al. 2024). This enables us to make comparison between the formation efficiencies of Gaia BHs and NSs.

From our simulations, we pick up compact binaries with the following criteria:

1. $10^2 \leq P/\text{day} \leq 10^4$, where P is a binary orbital period. This criterion may look loose, since the orbital periods of Gaia BHs and Gaia NSs are 100–4000 days, and 100–1000 days, respectively. Thus, we also investigate the case for $10^2 \leq P/\text{day} \leq 10^3$.
2. $m_2 \leq 1.1M_{\odot}$, where m_2 is a companion mass. This is because Gaia BH1, BH2, and NS1 have light companion stars: 0.93, 1.07, and $0.79M_{\odot}$, respectively. This is also true for Gaia BH3 and a large fraction of Gaia NSs.

3. Located outside of open clusters. None of Gaia BHs and Gaia NSs are located in open clusters.

Note that we do not put any constraints on orbital eccentricities in the above criteria. On the other hand, Gaia BHs and NS1 are characterized by moderately high eccentricities (0.5-0.7) and small (but non-zero) eccentricity (~ 0.1), respectively. Note that the eccentricities of Gaia NSs range from 0.1 to 0.8. Compact binaries we pick up may not be necessarily identified as Gaia BHs and NSs. Thus, these compact binaries are hereafter called “inert compact binaries”. They are also called “inert BH binaries (inert BHBs)” and “inert NS binaries (inert NSBs)” if they contain BHs and NSs, respectively.

3. RESULTS

First, We make clear whether inert BHBs and NSBs are formed from primordial binaries, or not. We find that no inert BHBs nor NSBs originate from primordial binaries in all our models other than the no-kick model. In the no-kick model, no inert BHBs originate from primordial binaries, while inert NSBs can be formed from primordial binaries and through dynamical interactions. Dynamical interactions play an important role in forming inert BHBs regardless of the presence of CCSN natal kicks. On the other hand, the formation of inert NSBs strongly depend on CCSN natal kicks. In section 3.1, we first investigate simulation results of models with CCSN natal kicks. In section 3.2, we compare simulation results of models with and without CCSN natal kicks.

3.1. Standard CCSN natal kicks

Figure 1 shows the formation efficiencies of inert BHBs and NSBs in all our cluster models other than the no-kick model. Inert BHBs with $10^2 \leq P/\text{day} \leq 10^4$ are formed at a formation efficiency of 10^{-6} - $10^{-5} M_{\odot}^{-1}$ except for the $f_{b, < 5 M_{\odot}} = 0$ model. This is consistent with previous results (Rastello et al. 2023; Tanikawa et al. 2024; Di Carlo et al. 2024). The formation efficiencies slowly increase with metallicity decreasing, initial cluster mass increasing, and initial half-mass density increasing. The reason for the dependence on initial cluster mass and half-mass density is that larger-mass, and higher-density clusters are harder to be disrupted in the Galactic tidal field, and thus these clusters have longer time to form inert BHBs. We describe the reason for the dependence on metallicity later. The formation efficiency in the $f_{b, < 5 M_{\odot}} = 0$ model is much smaller than those in the other models for the following reason. Generally, an inert BHB is formed, such that a single BH captures one star in a binary. Since the number of binaries in the $f_{b, < 5 M_{\odot}} = 0$ model is much smaller than those in the other models, inert BHBs are harder to form in the $f_{b, < 5 M_{\odot}} = 0$ model. Nevertheless, it is worth remarking that inert BHBs are formed at an efficiency of $\sim 10^{-7} M_{\odot}^{-1}$ even in the $f_{b, < 5 M_{\odot}} = 0$ model. They would be formed through triple-single encounters. This indicates that inert BHBs are robustly formed in open clusters, even if an initial binary fraction is extremely low. This is consistent with the results of Tanikawa et al. (2024).

Inert BHBs for $10^2 \leq P/\text{day} \leq 10^3$ are formed at an efficiency of 10^{-7} - $10^{-6} M_{\odot}^{-1}$. In the $M = 2000 M_{\odot}$ and $\rho = 200$ models, the number ratio of such inert BHBs to

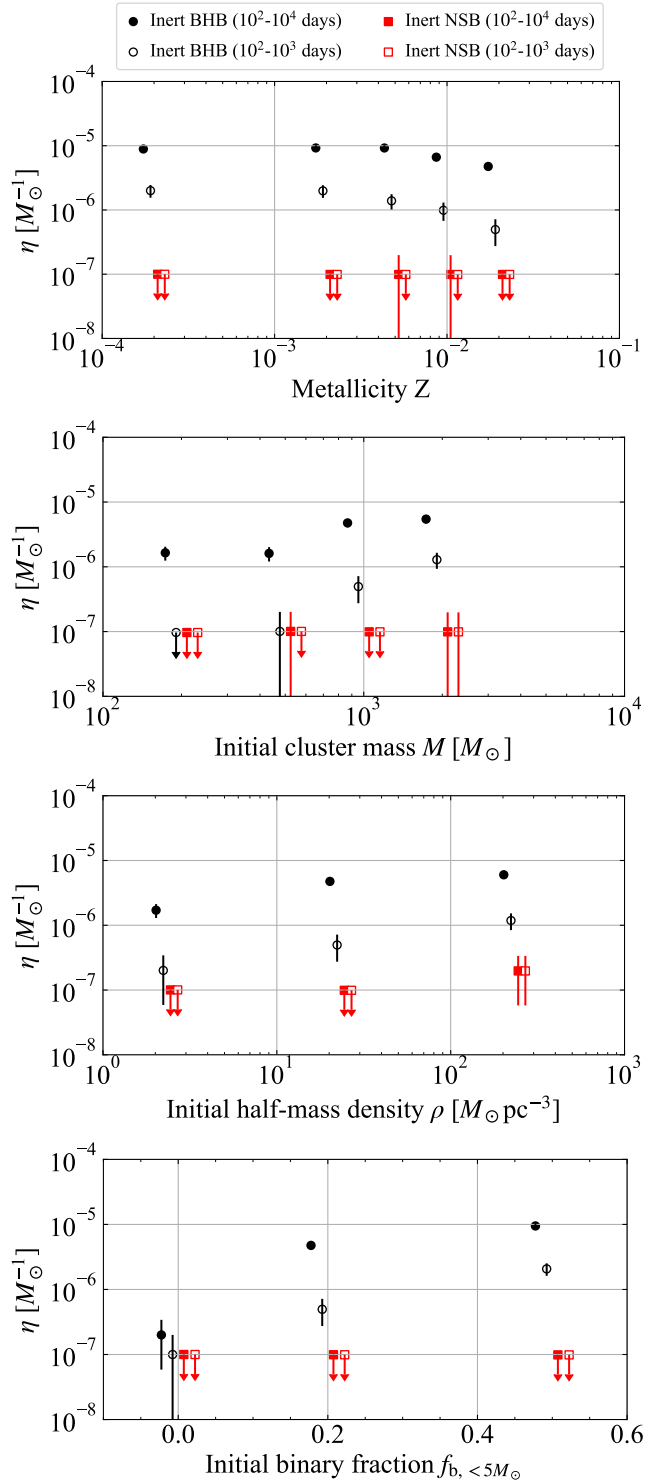


FIG. 1.— Formation efficiencies of inert BHBs (circles) and NSBs (squares) as a function of metallicity (Z), initial cluster mass (M), initial half-mass density (ρ), and initial binary fraction ($f_{b, < 5 M_{\odot}}$). Filled and open points show that the ranges of binary orbital periods are 10^2 - 10^4 days and 10^2 - 10^3 days, respectively. Circles and squares indicate inert BHBs and NSBs, respectively. These points are slightly shifted leftward or rightward for visibility. We calculate error bars, assuming that inert BHBs and NSBs are formed in Poisson process. Error bars in some models reach zero, since only one inert BHB or NSB is formed in these models. In several models, no inert NSBs are formed. For these models, we use down arrows to indicate the upper limits of inert NSB formation efficiencies.

all inert BHBs is large, more than 0.1. This would be because these clusters have larger escape velocities than the other models. A cluster with a larger escape velocity can retain closer binaries kicked by their dynamical interactions, and so make them closer and closer. Although the number ratio is also large in the $f_{b, < 5M_\odot} = 0$ model, we cannot identify if it is real, because the number of inert BHBs is too small.

The inert BHB formation efficiencies weakly increase with metallicities decreasing. The formation efficiency in the $Z = 0.0002$ model is 2 and 5 times than in the $Z = 0.02$ model for inert BHBs with $10^2 \leq P/\text{day} \leq 10^4$ and $10^2 \leq P/\text{day} \leq 10^3$, respectively. We look into the reason of the dependence on metallicity. This is because the dependence may be a key to elucidate the origin of Gaia BHs as discussed in El-Badry (2024b). Single BH formation efficiencies are not sensitive to metallicities: 2.7×10^{-3} , 2.8×10^{-3} , 2.9×10^{-3} , 3.2×10^{-3} , and $3.0 \times 10^{-3} M_\odot^{-1}$ for $Z = 0.02$, 0.01, 0.005, 0.002, and 0.0002 models, respectively. Metallicities do not affect cluster mass evolution: $\sim 700 M_\odot$, $\sim 200 M_\odot$ and $\lesssim 1 M_\odot$ at the clusters' ages of 40, 400, and 1000 Myrs, respectively, for all the metallicities. Thus, single BH formation efficiency and cluster mass evolution are not the reason for the dependence of the inert BHB formation efficiencies on metallicities. On the other hand, the average single BH masses are quite different among metallicities: 7.9, 11.7, 15.7, 17.4, and $20.3 M_\odot$ for $Z = 0.02$, 0.01, 0.005, 0.002, and 0.0002 models, respectively. Since more massive BHs can capture other stars more easily, single BH masses should strongly affect the dependence of the inert BHB formation efficiencies.

As seen in Figure 1, the formation efficiencies of inert BHBs weakly increase with increasing cluster mass. On the other hand, Figure 2 in Marín Pina et al. (2024) has shown that the formation efficiencies decrease with increasing cluster mass. This difference would come from two points. First, inert BHB formation is inhibited due to more pronounced dynamical heating by larger BH populations in more massive clusters, as pointed out by Kremer et al. (2018) and Marín Pina et al. (2024). The second point is as follows. For clusters with $\lesssim 10^3 M_\odot$, two-body relaxation (or thermal) timescale (Spitzer 1987) is sufficiently shorter than the Hubble time. Thus, BHs can interact with other stars for a long time with respect to clusters' thermal timescales. However, their interactions are prevented by tidal disruption of clusters. Since more massive clusters are more robust against the Galactic tidal field, they can form inert BHBs more efficiently. For clusters with $\gtrsim 10^5 M_\odot$, two-body relaxation time is comparable to or longer than the Hubble time. From the view point of clusters' thermal timescales, BHs have a shorter time to interact with other stars in more massive clusters. Note that the two-body relaxation time increases with increasing cluster mass. In fact, the number of BHs decreases more slowly with increasing cluster mass as seen in Figure 3 of Kremer et al. (2020), which have published the CMC models used by Marín Pina et al. (2024). This clearly indicates that clusters' thermal ages are younger and BHs have less chances to interact with other stars in more massive stars. About $10^4 M_\odot$ clusters may form inert BHs most efficiently, because they are hard to be tidally disrupted,

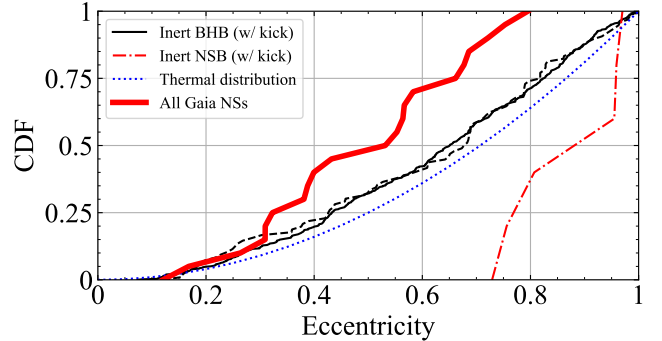


FIG. 2.— Cumulative eccentricity distribution of inert BHBs and NSBs. Solid and dashed curves indicate inert BHBs with binary orbital periods of 10^2 - 10^4 and 10^2 - 10^3 days, respectively. The dot dashed curve indicates inert NSBs in all the models. The thick solid curve indicates all the Gaia NSs. The dotted curve shows the thermal distribution.

and have a sufficiently shorter two-body relaxation time than the Hubble time.

In contrast to inert BHBs, inert NSBs are hardly formed. The number of inert NSBs is only 6 even if we put together all the models. It is only 3 for inert NSBs with $10^2 \leq P/\text{day} \leq 10^3$. If we weigh equally all the models, the formation efficiency is $6 \times 10^{-8} M_\odot^{-1}$ for all the inert NSBs, and $3 \times 10^{-8} M_\odot^{-1}$ for inert NSBs with $10^2 \leq P/\text{day} \leq 10^3$. The formation efficiency of inert NSBs is smaller than that of inert BHBs by at least an order of magnitude.

El-Badry et al. (2024b,a) have not fully ruled out the possibility that some of Gaia NSs are triple systems; for example NSs are actually double WDs. This motivates us to investigate triple and quadruple systems formed in all our cluster models. Such systems include an inner MS binary with a single NS as well as an inner double WDs with a single MS star. We do not find such a triple system. Instead, we find only one triple system which is potentially mistook for an inert NSB from the $Z = 0.0002$ model. Its inner binary consists of a $1.28 M_\odot$ NS and $0.022 M_\odot$ HeWD, and its period and eccentricity are 32 minutes and 0.023, respectively. This inner binary is formed from a primordial binary. The outer binary has the period and eccentricity of 560 days and 0.76, respectively, and the other outer component is a $0.95 M_\odot$ MS. The inner binary is in the process of mass transfer from the HeWD to the NS. This mass transfer is stable and long-lasting. This is the reason why the inner binary can capture the third star. Because of the mass transfer, the triple system should be observed as an X-ray binary, not as an inert NSB. Thus, we exclude the triple system from our list of inert NSBs. Even if we add it to our list, the formation efficiency of inert NSBs is still much smaller than that of inert BHBs.

Figure 2 shows the orbital eccentricity distribution of inert BHBs and NSBs. We put together inert BHBs and NSBs among all the models other than the no-kick model. We have to put together inert NSBs, because the number of inert NSBs is too small to statistically investigate the eccentricity distribution of inert NSBs for each model. We adopt the Kolmogorov-Smirnov (K-S) test to compare these distribution with the thermal distribution (Heggie 1975) and Gaia BHs and NSs. Note

TABLE 2
P-VALUES OF THE KOLMOGOROV-SMIRNOV (K-S) TEST FOR
ECCENTRICITY DISTRIBUTIONS OF INERT BHBs AND NSBs.

Binary type	Number	Comparison	P-value
Inert BHB (10^2 - 10^4 day)	556	Thermal	5.6×10^{-5}
Inert BHB (10^2 - 10^3 day)	97	Thermal	9.3×10^{-2}
Inert NSB (10^2 - 10^4 day)	6	Thermal	4.2×10^{-2}
Inert NSB selected	4	Thermal	1.4×10^{-1}
Inert NSB (no-kick)	34	Thermal	2.5×10^{-3}
Inert BHB (10^2 - 10^4 day)	556	Gaia BHs	6.4×10^{-1}
Inert BHB (10^2 - 10^3 day)	97	Gaia BHs	6.9×10^{-1}
Inert NSB (10^2 - 10^4 day)	6	Gaia NS1	2.9×10^{-1}
Inert NSB selected	4	Gaia NS1	4.0×10^{-1}
Inert NSB (no-kick)	34	Gaia NS1	5.7×10^{-2}
Inert NSB (10^2 - 10^4 day)	6	All Gaia NSs	1.9×10^{-4}
Inert NSB selected	4	All Gaia NSs	2.4×10^{-3}
Inert NSB (no-kick)	34	All Gaia NSs	1.0×10^{-5}

that Gaia BH1, BH2 and NS1 have orbital eccentricities of ~ 0.451 (El-Badry et al. 2023b), 0.518 (El-Badry et al. 2023c), and 0.124 (El-Badry et al. 2024b), respectively. After this paper was submitted, El-Badry et al. (2024a) have also published the orbital parameters of all Gaia NSs. We compare inert NSBs not only with Gaia NS1, but also with all the Gaia NSs. Table 2 shows the P-values of the K-S test. The eccentricity distribution of inert BHBs with $10^2 \leq P/\text{day} \leq 10^4$ is clearly more circular than the thermal distribution, since the P-value is 5.6×10^{-5} . This is possibly because eccentric BHBs are circularized by tidal interactions. This is also seen in the eccentricity-period diagram of binaries in Gaia DR3 (e.g. Gaia Collaboration et al. 2023b). On the other hand, the eccentricity distribution of inert BHBs with $10^2 \leq P/\text{day} \leq 10^3$ is not significantly different from the thermal distribution; the P-value is 9.3×10^{-2} . This may be due to their small number.

Although the eccentricity distribution of inert NSBs appears to be largely different from the thermal distribution, it is still consistent with the thermal distribution. The P-value is not small: 4.2×10^{-2} . This may be again due to the small statistics. As described later, the inert NSBs with the highest and second highest eccentricities are not formed through dynamical interactions (named “CCSN channel” later), although they are not primordial binaries. Moreover, these inert NSBs are formed only in the $\rho = 200$ model. A large fraction of open clusters in reality could be less dense than the $\rho = 200$ model. Thus, we construct inert NSBs, excluding these NSBs (“inert NSB selected” in Table 2). When we compare their eccentricity distribution with the thermal distribution, the P-value increases to 1.4×10^{-1} . It is natural that they are formed through dynamical interactions. Nevertheless, their eccentricity distribution may finally becomes more circular than the thermal distribution, similarly to inert BHBs, if we obtain more many inert NSBs with simulating more many clusters.

Inert BHBs and NSBs have the eccentricity distributions which are not inconsistent with Gaia BHs and Gaia NS1, respectively, regardless of how to choose these BHBs and NSBs. The P-values are more than 0.1. This may be due to the small numbers; the number of inert NSBs are only 6, and the numbers of Gaia BHs and Gaia NS1 are 2 and 1, respectively. In fact, when we compare our inert NSBs with all the Gaia NSs, the P-

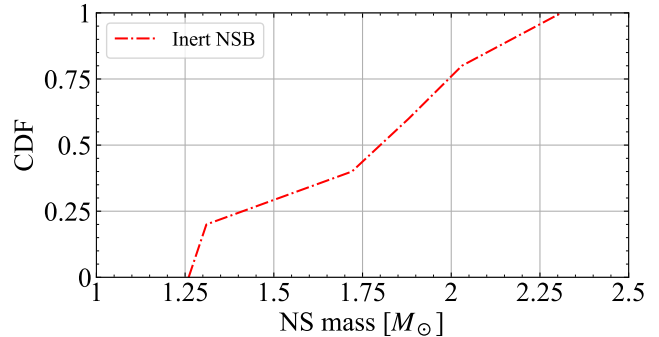


FIG. 3.— Cumulative NS mass distribution of inert NSBs in all the models.

values are quite small: 1.9×10^{-4} for all the inert NSBs, and 2.4×10^{-3} for the inert NSBs selected. Owing to the publication of Gaia NSs’ eccentricities, we can find that the eccentricity distribution of our inert NSBs is different from that of Gaia NSs. On the other hand, It seems that the eccentricity distribution of Gaia BHs is not currently helpful to assess if inert BHBs are identified as Gaia BHs.

Figure 3 shows the NS mass distribution of all the inert NSBs. 2 of the 6 inert NSBs have NSs with $> 2M_\odot$. These NSs are formed through AIC of WD merger products (called “AIC channel” later). The detail formation channel is described below.

Hereafter, we describe three formation channels of inert NSBs. These channels are illustrated in Figures 4, 5, and 6. In the first channel, NSs are formed through AIC of WD merger products. We call this channel “AIC channel”. We explain the AIC channel along with Figure 4. This channel starts with a primordial binary consisting of intermediate mass stars: 6.2 and $5.1M_\odot$ MSs. They evolve to a close double WDs with $1.2M_\odot$ ONeWD and $0.81M_\odot$ COWD via common envelope evolution. They merge through orbital decay due to gravitational wave radiation. The merger product avoids type Ia SN explosion, and collapses to a NS (AIC). The NS mass is $> 2M_\odot$. The NS can avoid escaping from the open cluster, since AIC generate no natal kick in our model. Finally, the NS dynamically interacts with another primordial binary, and captures one star of the primordial binary. The resulting NSB has orbital period and eccentricity of ~ 1800 day and ~ 0.76 , respectively. This happens in the $Z = 0.005$ model. Another one also occurs in the $M = 2000M_\odot$ model.

Our simulations implement a NS formation channel through AIC of WDs accreting from non-degenerate companions. In fact, we find such NS formations. However, they do not evolve to inert NSBs. Their orbital periods are much shorter than 10^2 days, because such NS formations involve mass transfer from non-degenerate companions. These binaries are too close to interact with other stars dynamically. Moreover, if they experience dynamical interactions, their orbital periods will be still much shorter than 10^2 days. Such tight binaries tend to become tighter through dynamical interactions.

The second channel involves ECSNe as seen in Figure 5. We call this channel “ECSN channel”. We find this channel in the $Z = 0.01$ and $M = 500M_\odot$ models. Here, we introduce the formation processes of the inert NSB in the former model (see also Figure 5). A $7.5M_\odot$ MS

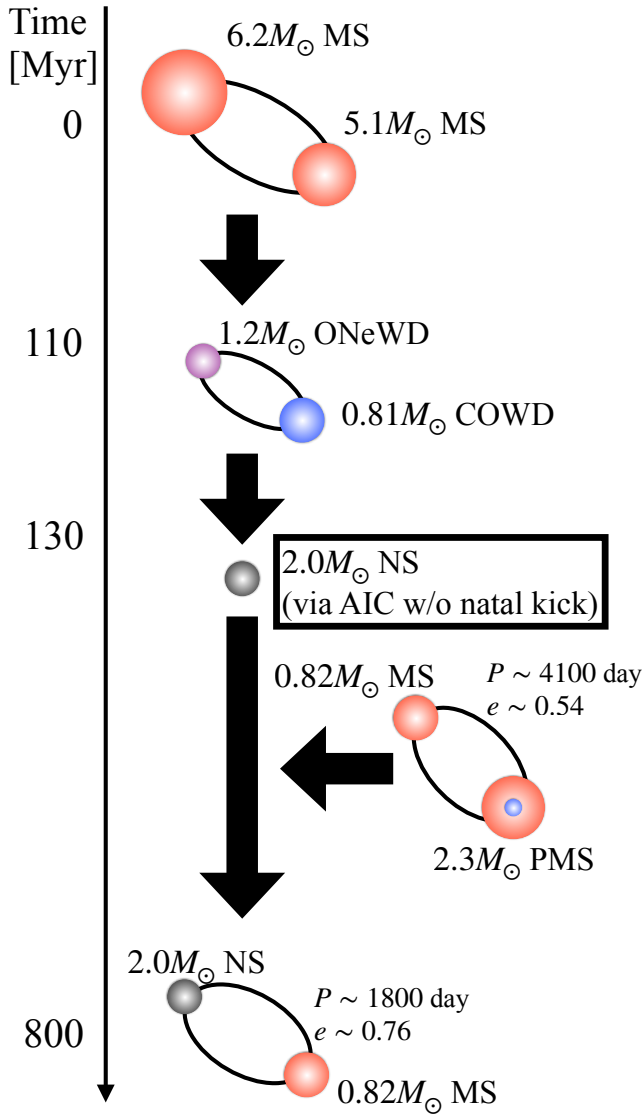


FIG. 4.— Inert NSB formation channel via AIC. This happens in model $Z = 0.005$. A binary with 6.2 and $5.1M_{\odot}$ MSs evolves to binary WDs with $1.2M_{\odot}$ ONeWD and $0.81M_{\odot}$ COWD. These WDs merge, and its merger product collapses to a NS. Because this NS receives no natal kick, it stays inside of the open cluster. The NS closely interacts with a binary with $0.82M_{\odot}$ MS and $2.3M_{\odot}$ PMS, and capture the $0.82M_{\odot}$ MS, resulting in an inert NSB. It finally escapes from the open cluster.

with a $6.3M_{\odot}$ MS companion evolves to a $1.3M_{\odot}$ NS via ECSN. Because of ECSN, the NS receives a small kick velocity (3.5 km s^{-1}), and is not ejected from the open cluster. Its companion evolves to a $1.2M_{\odot}$ ONeWD. This binary experiences no interaction any more, since their separation is large. Very later, this binary interacts with another binary with 0.33 and $0.70M_{\odot}$ MSs. This interaction raises an inert NSB with the $1.3M_{\odot}$ NS and $0.33M_{\odot}$ MS. Note that, although a lower-mass star is harder to be took as a binary member, it is not impossible. This has orbital period and eccentricity of ~ 1100 day and 0.73 , respectively.

In the third channel, NSs arise from CCSNe. Thus, we refer to them as “CCSN channel”. We obtain two inert NSBs, both of which are formed in the $\rho = 200$ model.

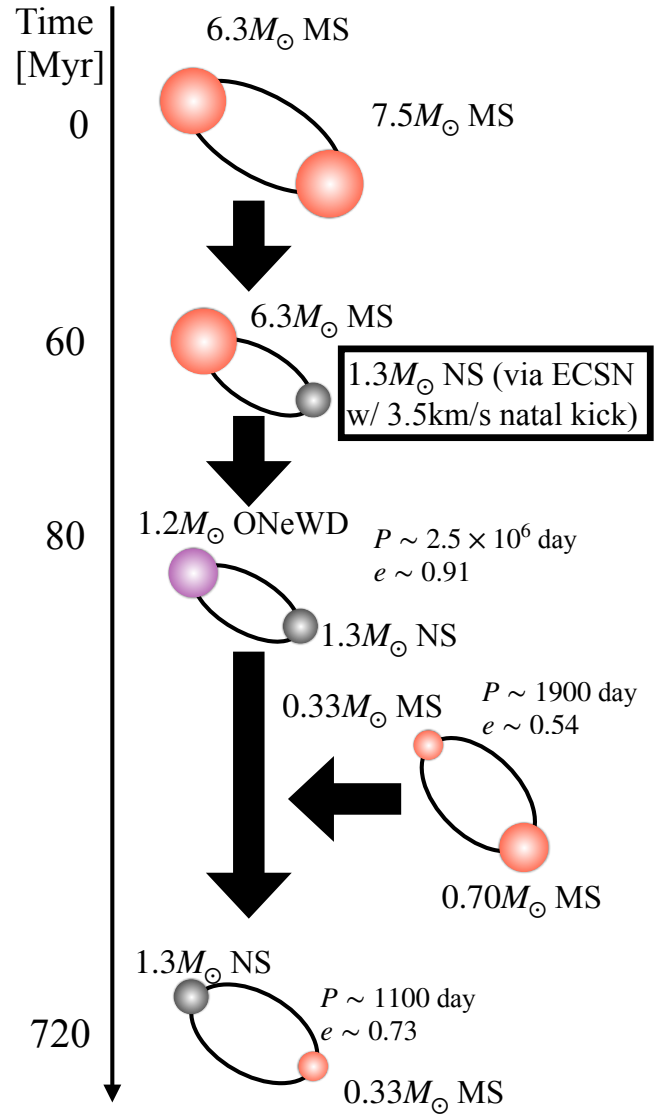


FIG. 5.— Inert NSB formation channel via ECSN. This happens in model $Z = 0.01$. A binary with 7.5 and $6.3M_{\odot}$ MSs evolves to a binary with $1.3M_{\odot}$ NS and $1.2M_{\odot}$ ONeWD. The NS receives a small kick (3.5 km s^{-1}) because of ECSN, and is retained in the open cluster. The binary interacts with a binary with 0.70 and $0.33M_{\odot}$ MSs, and leaves an inert NSB consisting of the NS and $0.33M_{\odot}$ MS. The inert NSB finally escapes from the open cluster.

In Figure 6, we show the formation pathway of one of the two. This channel begins with a primordial binary with 18 and $17M_{\odot}$ MSs. The primordial binary merges to a $35M_{\odot}$ MS. Just after the merger, the $35M_{\odot}$ MS soon captures a $0.75M_{\odot}$ MS. It evolves to a $32M_{\odot}$ PMS, and experiences common envelope evolution with its $0.75M_{\odot}$ MS companion. The common envelope evolution leaves a short-period (2.8 day) binary with a $6.8M_{\odot}$ He star and $0.75M_{\odot}$ MS. The He star causes a CCSN with a kick velocity of 260 km s^{-1} . It luckily survives as a binary. Such a close binary can survive a CCSN depending on the kick velocity direction despite of CCSN mass loss, because its binary internal motion has large velocity comparable to the kick velocity. However, the natal kick greatly affects the center-of-mass velocity of the binary, and ejects the resulting NSB from the open cluster.

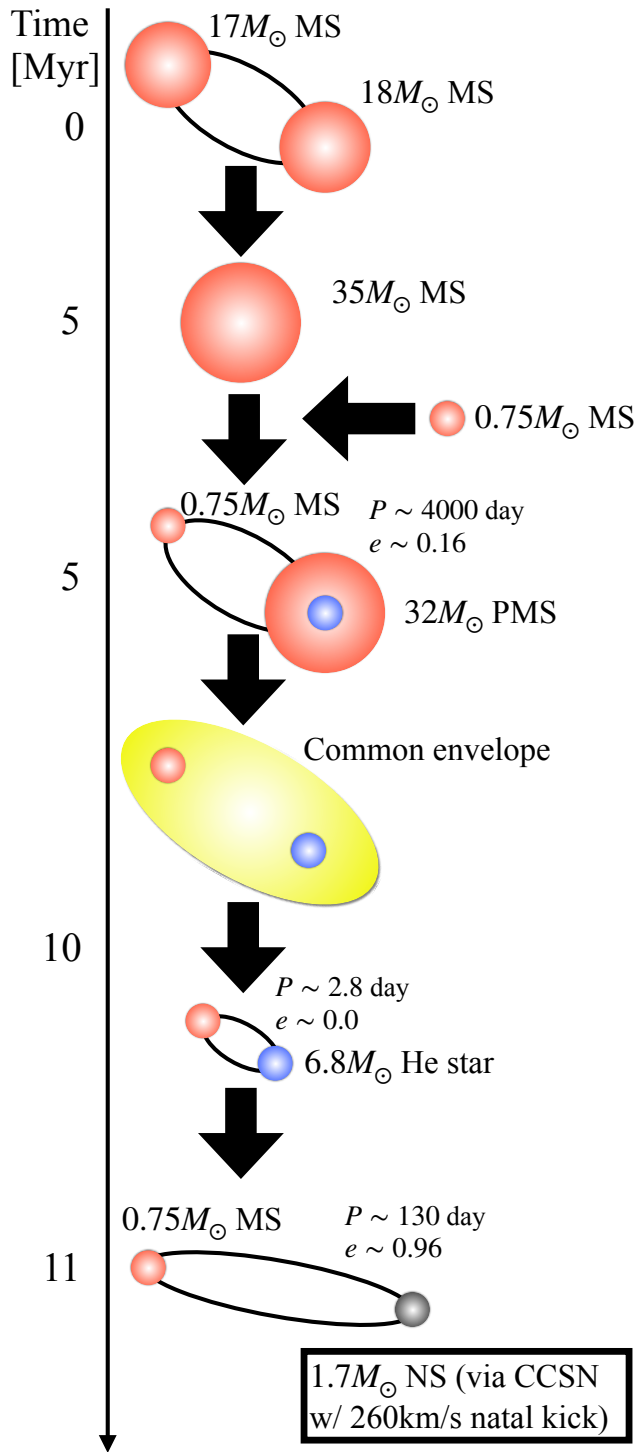


FIG. 6.— Inert NSB formation channel via CCSN. This happens in model $\rho = 200$. A binary with 18 and $17M_{\odot}$ MSs merges to a $35M_{\odot}$ MS. The $35M_{\odot}$ MS soon captures a $0.75M_{\odot}$ MS. This binary experiences common envelope evolution, and results in a close binary with $6.8M_{\odot}$ He star and $0.75M_{\odot}$ MS. The He star undergoes CCSN, and creates a $1.7M_{\odot}$ NS. Although the NS receives a large kick (260 km s^{-1}), the binary is not disrupted because of the close separation, and becomes an inert NSB. On the other hand, the large kick ejects the inert NSB from the open cluster.

The CCSN channel involves a dynamical interaction to form the progenitors of inert NSBs, while the final configurations of inert NSBs are dependent on binary physics, not on dynamical interactions. Furthermore, this channel tends to inert NSBs with high eccentricities. In fact, the two NSBs formed through the CCSN channel have the highest and second highest eccentricities among inert NSBs in all our models other than the no-kick model. Thus, we exclude inert NSBs via the CCSN channel from the “inert NSBs selected” in Table 2 when we compare their eccentricity distribution with the thermal distribution.

The CCSN channel appears only in the $\rho = 200$ model. We interpret the reason as follows. This channel requires a post common envelope binary consisting of $\leq 1.1M_{\odot}$ MS star and massive He star (say $\gtrsim 3M_{\odot}$). If a He star has $\lesssim 3M_{\odot}$, such a post common envelope binary cannot become wide enough to be an inert NSB after the He star collapses to a NS. This is because the He star does not lose its mass during its CCSN. The kick velocity is at most comparable to the velocity of the binary internal motion, and thus cannot change the binary period largely. A He star with $\gtrsim 3M_{\odot}$ is raised by a $\gtrsim 11M_{\odot}$ MS. However, our initial conditions prohibit primordial binaries with $\gtrsim 11M_{\odot}$ and $\lesssim 1.1M_{\odot}$ MS stars, since the minimum binary mass ratio is 0.1. Thus, binaries with $\gtrsim 11M_{\odot}$ and $\lesssim 1.1M_{\odot}$ MS stars need to be formed through dynamical interactions before $\gtrsim 11M_{\odot}$ stars evolve to NSs or BHs. Dynamical interactions in the $\rho = 200$ model are the most active among all our models because of its high density. Thus, many binaries with $\gtrsim 11M_{\odot}$ and $\lesssim 1.1M_{\odot}$ MS stars are formed, and there are many chances to achieve the CCSN channel in the $\rho = 200$ model. We have to note that this reason strongly depends on our initial conditions in which there are no primordial binaries with $\gtrsim 11M_{\odot}$ and $\lesssim 1.1M_{\odot}$ MS stars. It would not be strange if the CCSN channel is achieved in real open clusters with the initial half-mass density of $< 200M_{\odot} \text{ pc}^{-3}$.

If we reduce the minimum binary mass ratio, another inert NSB formation channel (hereafter called primordial binary or PB channel) similar to the CCSN channel may appear in primordial binaries, and in isolated binaries. The difference between the two channels is how to form progenitors of inert NSBs. The progenitors are formed through dynamical interactions in the CCSN channel, while they are present from the initial time in the PB channel. The PB channel increases the formation efficiency of inert NSBs (possibly BHBs) not only in open clusters, but also on isolated fields. In this case, the importance of open clusters would diminish. This is because the number of channels increases from 3 to 4 in open clusters, while it increases from 0 to 1 on isolated fields.

3.2. Effects of CCSN natal kicks

Hereafter, we investigate the effects of CCSN natal kicks, showing the simulation results of the no-kick model. Figure 7 shows the formation efficiency of inert BHBs and NSBs in the $Z = 0.002$ and no-kick models. The formation efficiency of inert BHBs in the no-kick model is similar to that in the other models regardless of $10^2 \leq P/\text{day} \leq 10^4$ and $10^2 \leq P/\text{day} \leq 10^3$. On the other hand, NSBs are formed much more efficiently in

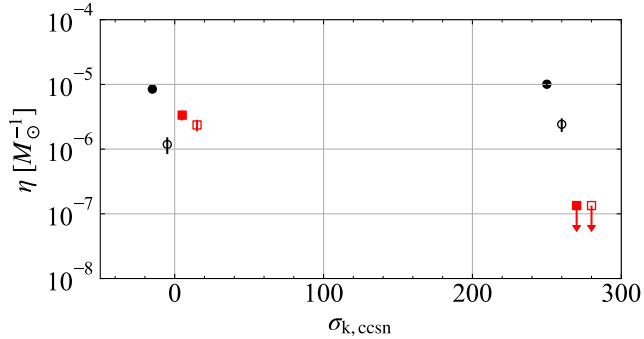


FIG. 7.— The same as Figure 1 except for a function of CCSN natal kick velocity ($\sigma_{k,ccsn}$). The results of $Z = 0.002$ and no-kick models are shown.

the no-kick model (a few $10^{-6} M_{\odot}^{-1}$) than in the other models ($\lesssim 10^{-7} M_{\odot}^{-1}$). There are 34 inert NSBs with $10^2 \leq P/\text{day} \leq 10^4$. 25 of them originate from primordial binaries, and the rest of them are formed through dynamical interactions.

The no-kick model has a high formation efficiency of inert NSBs, in contrast to other models. As described above, a dominant fraction of inert NSBs ($\sim 70\%$) originate from primordial binaries. We describe their formation pathway here. We do not illustrate it, because we suppose the no-kick model is unrealistic. Let's prepare a binary with $\sim 8 M_{\odot}$ and $\sim 1 M_{\odot}$ MSs. Its separation is $\sim 3 \times 10^3 R_{\odot}$. The heavier star evolves to a PMS, and fills its Roche lobe. Then, the binary experiences common envelope evolution. The common envelope evolution leaves a binary with $\sim 2 M_{\odot}$ He star and $\sim 1 M_{\odot}$ MS star. It is separated by $\sim 40 R_{\odot}$. The He star causes a CCSN, and leaves behind a NS. Because of CCSN mass loss, the binary is widened, and fits in an inert NSB. In all the models with CCSN natal kicks, such inert NSBs cannot be formed. CCSN natal kicks disrupt the binary at a high probability. Just before CCSNe, the velocities of binary internal motions have $\sim 100 \text{ km s}^{-1}$, much smaller than CCSN natal kick velocities (265 km s^{-1}).

9 of 34 inert NSBs are dynamically formed. For 6 of them, NSs capture their companions. On the other hand, for the rest of them, NS progenitors capture their companions, and later they collapse to NSs. The latter formation pathway is the same as the formation pathway from primordial binaries described above, except that a binary with $\sim 8 M_{\odot}$ and $\sim 1 M_{\odot}$ MSs is formed through dynamical interactions.

Figure 8 shows the cumulative eccentricity distribution of inert NSBs in the no-kick model. Their orbital eccentricities appear to deviate from the thermal distribution. In fact, the deviation is significant; the P-value of the K-S test is 2.5×10^{-3} as seen in Table 2. This is because a dominant fraction of these inert NSBs originate from primordial binaries, not formed through dynamical interactions. On the other hand, the eccentricity distribution of these NSBs is not significantly different from Gaia NS1; the P-value is 5.7×10^{-2} . This shows that it is difficult to distinguish the differences among these eccentricity distributions due to the small statistics if we use only Gaia NS1. However, when we use all the Gaia NSs, the P-value is small, 1.0×10^{-5} . Because of improved statistics, we can conclude that the eccentricity distribu-

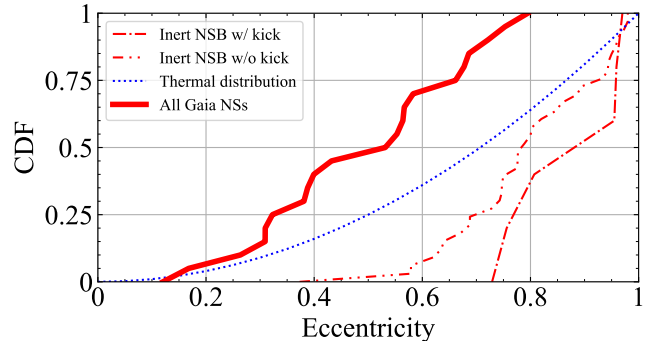


FIG. 8.— Cumulative eccentricity distribution of inert NSBs in all models except for the no-kick model (Inert NSB w/ kick), and in the no-kick model (Inert NSB w/o kick). The thick solid curve indicates all the Gaia NSs. The dotted curve shows the thermal distribution.

tion of inert NSBs in the no-kick model is different from that of all Gaia NSs.

When we switch off CCSN natal kicks, the number of NSs retained in open clusters should increase by about 100 times. Nevertheless, the number of inert NSBs dynamically formed is still low for the following reason. NSs are hard to capture other stars dynamically, because their masses are comparable to or less than surrounding main-sequence (MS) stars. Note that the lifetime of a $1.4 M_{\odot}$ MS star is a few Gyr, which is longer than the lifetime of open clusters.

4. DISCUSSION

First, we discuss whether inert BHBs and NSBs correspond to Gaia BHs and NSs, respectively. Here, we do not consider the simulation results of the no-kick model. As seen in Table 2, the P-values of the K-S test do not show that inert BHBs have different orbital eccentricities from Gaia BHs. The eccentricity distributions of inert NSBs with $10^2 \leq P/\text{day} \leq 10^4$ and inert NSBs selected in Table 2 are not inconsistent with Gaia NS1's eccentricity. However, when we consider all the Gaia NSs, the eccentricity distribution of inert NSBs is different from that of all Gaia NSs. Thus, it is difficult to identify our inert NSBs as Gaia NSs.

Even if we identify our inert NSBs as Gaia NSs, there is another problem. We compare the formation efficiencies of inert BHBs and NSBs, assuming that inert NSBs correspond to Gaia NSs. The formation efficiency of inert NSBs is smaller than that of inert BHBs by two or more orders of magnitude except for the no-kick model (see Figure 1). However, the number of discovered Gaia NSs, 21 (El-Badry et al. 2024b,a), is much larger than the number of Gaia BHs, 2. This shows that open clusters cannot form enough Gaia NSs to be already discovered.

This is also true for the no-kick model. As for inert BHBs and NSBs with $10^2 \leq P/\text{day} \leq 10^4$, the formation efficiency of inert NSBs is smaller than that of inert BHBs. Actually, the formation efficiency of inert NSBs with $10^2 \leq P/\text{day} \leq 10^3$ is larger than that of inert BHBs with $10^2 \leq P/\text{day} \leq 10^3$. However, a dominant fraction of inert NSB formed in the no-kick model ($\sim 74\%$) originate from primordial binaries. This means that such inert NSBs can be formed through isolated binary evolution if CCSN natal kicks are smaller than expected. In this case, although a large number of inert NSBs can be

formed in open clusters, inert NSBs are also formed more efficiently on isolated fields. Thus, open clusters cannot dominate the formation of Gaia NSs, even if CCSN natal kicks are unrealistically small.

It is unclear how efficiently Gaia (Gaia Collaboration et al. 2023b) and its spectroscopic follow-up observations (El-Badry et al. 2023b,c, 2024b,a; Chakrabarti et al. 2023; Gaia Collaboration et al. 2024) can discover Gaia BHs and NSs. Thus, the numbers of discovered Gaia BHs and NSs do not directly mean their intrinsic numbers. However, for the following reason, we infer that Gaia NSs are harder to be discovered than Gaia BHs, and that the intrinsic number of Gaia NSs should be much larger than that of Gaia BHs. All Gaia and its follow-up observations search for Gaia BHs and NSs, observing BHs' and NSs' companions. Because such companions are swayed more largely with BH and NS masses increasing, Gaia, astrometric observations, can more easily discover BHs and NSs with larger masses. Similarly, companions tend to have larger radial velocity variations, and thus spectroscopic follow-up observations can detect more massive BHs and NSs more efficiently. Since NSs are generally less massive than BHs, the intrinsic number ratio of Gaia NSs to Gaia BHs should be larger than the reported number ratio. As seen in section 3, open clusters form Gaia BHs more efficiently than Gaia NSs. This is in contrast to the observational results. Eventually, open clusters cannot form both of Gaia BHs and Gaia NSs.

As described above, Gaia NSs are unlikely to be formed in open clusters. Nevertheless, we do not mean that Gaia BHs are not formed in open clusters. The formation efficiency of Gaia BHs in $\sim 10^3 M_\odot$ open clusters is still high ($\sim 10^{-6}$ - $10^{-5} M_\odot$), if we do not adopt unrealistically small half-mass density ($\rho \sim 2 M_\odot \text{ pc}^{-3}$) nor unrealistically small binary fraction ($f_{b,<5M_\odot} \sim 0$). It is reasonable that open clusters have $\rho \gtrsim 20 M_\odot \text{ pc}^{-3}$ initially. Note that, although nearby open clusters have $\rho \sim 10^{-2}$ - $10^2 M_\odot \text{ pc}^{-3}$, they should become less dense with time through gas expulsion, stellar evolution mass loss, and two-body relaxation (Portegies Zwart et al. 2010). Initial binary fractions in open clusters should be $f_{b,<5M_\odot} \gtrsim 0.2$, similarly to isolated fields (Sana et al. 2012; Moe & Di Stefano 2017). It would be possible that Gaia BHs are formed in open clusters, while Gaia NSs (El-Badry et al. 2024b) and ultramassive WDs (Yamaguchi et al. 2024) are formed on isolated fields. This will become clear after much more Gaia BHs will be discovered.

5. SUMMARY

We have performed gravitational N -body simulations for $1.3 \times 10^8 M_\odot$ open clusters in total with various masses, metallicities, densities, binary fractions, and natal kick velocities. We have found that the formation efficiency is 10^{-6} - $10^{-5} M_\odot^{-1}$ for Gaia BHs in open clusters with realistic parameters, while $\lesssim 10^{-7} M_\odot^{-1}$ for Gaia NSs. This is in contrast to observational results in which

the number of discovered Gaia BHs (3) is smaller than that of Gaia NSs (21). Moreover, inert NSBs obtained from our simulations have different orbital eccentricities from Gaia NSs. Note that inert BHBs obtained from our simulations have orbital eccentricities not inconsistent with Gaia BHs. This is partly because of the small statistics for Gaia BHs.

We have switched off CCSN natal kicks in order to increase the number of NSs retained in open clusters. Although we expected the number of inert NSBs to increase, the formation efficiency of inert NSBs is at most comparable to that of inert BHBs. NSs are much harder to capture companions than BHs, since NSs are not so heavier than MSs and WDs during open cluster lifetimes (~ 1 Gyr). Moreover, a dominant fraction of them are formed from primordial binaries. Thus, inert NSBs are less efficiently formed in open clusters than on isolated fields, even if CCSNe generate no natal kicks.

Regardless of the presence and absence of CCSN natal kicks, inert NSBs are formed in open clusters less efficiently than, or at most comparable to inert BHBs. Additionally, if there are no CCSN natal kicks, inert NSBs are formed more efficiently on isolated fields than in open clusters. Thus, we have concluded that open clusters cannot form both Gaia BHs and NSs. However, we do not mean that open clusters cannot form Gaia BHs. It would be possible that Gaia BHs are formed in open clusters, while Gaia NSs are formed on isolated fields. We will make it clear when more many Gaia BHs will be discovered in the future.

ACKNOWLEDGMENTS

This research could not be accomplished without the support by Grants-in-Aid for Scientific Research (19K03907, 24K07040) from the Japan Society for the Promotion of Science. M.F. is supported by The University of Tokyo Excellent Young Researcher Program. L.W. thanks the support from the one-hundred-talent project of Sun Yat-sen University, the Fundamental Research Funds for the Central Universities, Sun Yat-sen University (22hytd09) and the National Natural Science Foundation of China through grant 12073090 and 12233013. Numerical simulations are carried out on Small Parallel Computers at Center for Computational Astrophysics, National Astronomical Observatory of Japan, the Yukawa Institute Computer Facility, and Cygnus/Pegasus at the CCS, University of Tsukuba.

DATA AVAILABILITY

Results will be shared on reasonable request to authors. The data is generated by the software PeTar and SDAR, which are available in GitHub at <https://github.com/lwang-astro/PeTar> and <https://github.com/lwang-astro/SDAR>, respectively. The initial conditions of star cluster models are generated by the software MCLUSTER (Küpper et al. 2011), which is available in GitHub at <https://github.com/lwang-astro/mcluster>.

REFERENCES

- Abbott B. P., et al., 2019, *Physical Review X*, 9, 031040
 Abbott R., et al., 2021, *Physical Review X*, 11, 021053
 Abbott R., et al., 2023, *Physical Review X*, 13, 011048
 Abdikamalov E. B., Ott C. D., Rezzolla L., Dessart L., Dimmelmeyer H., Marek A., Janka H. T., 2010, *Phys. Rev. D*, 81, 044012

- Abdul-Masih M., et al., 2020, *Nature*, 580, E11
- Andrews J. J., Taggart K., Foley R., 2022, arXiv e-prints, p. arXiv:2207.00680
- Balbinot E., et al., 2024, arXiv e-prints, p. arXiv:2404.11604
- Banerjee S., Belczynski K., Fryer C. L., Berczik P., Hurley J. R., Spurzem R., Wang L., 2020, *A&A*, 639, A41
- Baron E., Cooperstein J., Kahana S., Nomoto K., 1987, *ApJ*, 320, 304
- Belloni D., Askar A., Giersz M., Kroupa P., Rocha-Pinto H. J., 2017, *MNRAS*, 471, 2812
- Bodensteiner J., et al., 2020, *A&A*, 641, A43
- Bovy J., 2015, *ApJS*, 216, 29
- Casares J., Jonker P. G., Israelian G., 2017, *X-Ray Binaries*, p. 1499, doi:10.1007/978-3-319-21846-5_111
- Chakrabarti S., et al., 2023, *AJ*, 166, 6
- Chawla C., Chatterjee S., Breivik K., Moorthy C. K., Andrews J. J., Sanderson R. E., 2022, *ApJ*, 931, 107
- Claeys J. S. W., Pols O. R., Izzard R. G., Vink J., Verbunt F. W. M., 2014, *A&A*, 563, A83
- Dan M., Rosswog S., Brüggen M., Podsiadlowski P., 2014, *MNRAS*, 438, 14
- Dessart L., Burrows A., Ott C. D., Livne E., Yoon S. C., Langer N., 2006, *ApJ*, 644, 1063
- Di Carlo U. N., Agrawal P., Rodriguez C. L., Breivik K., 2024, *ApJ*, 965, 22
- El-Badry K., 2024a, arXiv e-prints, p. arXiv:2403.12146
- El-Badry K., 2024b, arXiv e-prints, p. arXiv:2404.13047
- El-Badry K., Burdge K. B., 2022, *MNRAS*, 511, 24
- El-Badry K., Quataert E., 2020, *MNRAS*, 493, L22
- El-Badry K., Quataert E., 2021, *MNRAS*, 502, 3436
- El-Badry K., Burdge K. B., Mróz P., 2022a, *MNRAS*, 511, 3089
- El-Badry K., Seeburger R., Jayasinghe T., Rix H.-W., Almada S., Conroy C., Price-Whelan A. M., Burdge K., 2022b, *MNRAS*, 512, 5620
- El-Badry K., et al., 2023a, *The Open Journal of Astrophysics*, 6, 28
- El-Badry K., et al., 2023b, *MNRAS*, 518, 1057
- El-Badry K., et al., 2023c, *MNRAS*, 521, 4323
- El-Badry K., et al., 2024a, arXiv e-prints, p. arXiv:2405.00089
- El-Badry K., et al., 2024b, *The Open Journal of Astrophysics*, 7, 27
- Ferrand G., Tanikawa A., Warren D. C., Nagataki S., Safi-Harb S., Decourchelle A., 2022, *ApJ*, 930, 92
- Fryer C., Benz W., Herant M., Colgate S. A., 1999, *ApJ*, 516, 892
- Fryer C. L., Belczynski K., Wiktorowicz G., Dominik M., Kalogera V., Holz D. E., 2012, *ApJ*, 749, 91
- Gaia Collaboration et al., 2023a, *A&A*, 674, A1
- Gaia Collaboration et al., 2023b, *A&A*, 674, A34
- Gaia Collaboration et al., 2024, arXiv e-prints, p. arXiv:2404.10486
- Geier S., Dorsch M., Dawson H., Pelisoli I., Munday J., Marsh T. R., Schaffenroth V., Heber U., 2023, *A&A*, 677, A11
- Generozov A., Perets H. B., 2023, arXiv e-prints, p. arXiv:2312.03066
- Gessner A., Janka H.-T., 2018, *ApJ*, 865, 61
- Giesers B., et al., 2018, *MNRAS*, 475, L15
- Gronow S., Collins C., Ohlmann S. T., Pakmor R., Kromer M., Seitenzahl I. R., Sim S. A., Röpké F. K., 2020, *A&A*, 635, A169
- Guillochon J., Dan M., Ramirez-Ruiz E., Rosswog S., 2010, *ApJ*, 709, L64
- Heggie D. C., 1975, *MNRAS*, 173, 729
- Hirai R., Mandel I., 2022, *ApJ*, 937, L42
- Hobbs G., Lorimer D. R., Lyne A. G., Kramer M., 2005, *MNRAS*, 360, 974
- Howl K., et al., 2024, *Uncovering the Invisible: A Study of Gaia18ajz, a Candidate Black Hole Revealed by Microlensing* (arXiv:2403.09006)
- Hurley J. R., Pols O. R., Tout C. A., 2000, *MNRAS*, 315, 543
- Hurley J. R., Tout C. A., Pols O. R., 2002, *MNRAS*, 329, 897
- Iorio G., et al., 2024, arXiv e-prints, p. arXiv:2404.17568
- Ivanova N., Heinke C. O., Rasio F. A., Belczynski K., Fregeau J. M., 2008, *MNRAS*, 386, 553
- Iwasawa M., Tanikawa A., Hosono N., Nitadori K., Muranushi T., Makino J., 2016, *PASJ*, 68, 54
- Iwasawa M., Oshino S., Fujii M. S., Hori Y., 2017, *PASJ*, 69, 81
- Iwasawa M., Namekata D., Nitadori K., Nomura K., Wang L., Tsubouchi M., Makino J., 2020, *PASJ*, 72, 13
- Jayasinghe T., et al., 2021, *MNRAS*, 504, 2577
- Jayasinghe T., et al., 2022, *MNRAS*, 516, 5945
- Jayasinghe T., Rowan D. M., Thompson T. A., Kochanek C. S., Stanek K. Z., 2023, *MNRAS*, 521, 5927
- Jones S., et al., 2013, *ApJ*, 772, 150
- Kashyap R., Fisher R., García-Berro E., Aznar-Siguán G., Ji S., Lorén-Aguilar P., 2015, *ApJ*, 800, L7
- Kashyap R., Haque T., Lorén-Aguilar P., García-Berro E., Fisher R., 2018, *ApJ*, 869, 140
- Kotko I., Banerjee S., Belczynski K., 2024, arXiv e-prints, p. arXiv:2403.13579
- Kremer K., Ye C. S., Chatterjee S., Rodriguez C. L., Rasio F. A., 2018, *ApJ*, 855, L15
- Kremer K., et al., 2020, *ApJS*, 247, 48
- Kremer K., Fuller J., Piro A. L., Ransom S. M., 2023, *MNRAS*, 525, L22
- Kroupa P., 1995a, *MNRAS*, 277, 1491
- Kroupa P., 1995b, *MNRAS*, 277, 1507
- Kroupa P., 2001, *MNRAS*, 322, 231
- Küpper A. H. W., Maschberger T., Kroupa P., Baumgardt H., 2011, *MNRAS*, 417, 2300
- Lam C. Y., et al., 2022, *ApJ*, 933, L23
- Lennon D. J., Dufton P. L., Villaseñor J. I., Evans C. J., Langer N., Saxton R., Monageng I. M., Toonen S., 2022, *A&A*, 665, A180
- Liu J., et al., 2019, *Nature*, 575, 618
- Longo Micchi L. F., Radice D., Chirenti C., 2023, *MNRAS*, 525, 6359
- Marín Pina D., Rastello S., Gieles M., Kremer K., Fitzgerald L., Rando B., 2024, arXiv e-prints, p. arXiv:2404.13036
- Miyaji S., Nomoto K., Yokoi K., Sugimoto D., 1980, *PASJ*, 32, 303
- Moe M., Di Stefano R., 2017, *ApJS*, 230, 15
- Mori M., Sawada R., Suwa Y., Tanikawa A., Kashiwara K., Murase K., 2023, arXiv e-prints, p. arXiv:2306.17381
- Nomoto K., 1982, *ApJ*, 257, 780
- Nomoto K., 1984, *ApJ*, 277, 791
- Nomoto K., 1987, *ApJ*, 322, 206
- Nomoto K., Kondo Y., 1991, *ApJ*, 367, L19
- Oshino S., Funato Y., Makino J., 2011, *PASJ*, 63, 881
- Pakmor R., Kromer M., Röpké F. K., Sim S. A., Ruitter A. J., Hillebrandt W., 2010, *Nature*, 463, 61
- Pakmor R., Hachinger S., Röpké F. K., Hillebrandt W., 2011, *A&A*, 528, A117
- Pakmor R., Edelmann P., Röpké F. K., Hillebrandt W., 2012a, *MNRAS*, 424, 2222
- Pakmor R., Kromer M., Taubenberger S., Sim S. A., Röpké F. K., Hillebrandt W., 2012b, *ApJ*, 747, L10
- Pakmor R., Kromer M., Taubenberger S., Springel V., 2013, *ApJ*, 770, L8
- Pakmor R., Zenati Y., Perets H. B., Toonen S., 2021, *MNRAS*, 503, 4734
- Perets H. B., et al., 2010, *Nature*, 465, 322
- Phillippov A., Kramer M., 2022, *ARA&A*, 60, 495
- Podsiadlowski P., Langer N., Poelarends A. J. T., Rappaport S., Heger A., Pfahl E., 2004, *ApJ*, 612, 1044
- Portegies Zwart S. F., McMillan S. L. W., Gieles M., 2010, *ARA&A*, 48, 431
- Rastello S., Iorio G., Mapelli M., Arca-Sedda M., Di Carlo U. N., Escobar G. J., Shenar T., Torniamenti S., 2023, *MNRAS*, 526, 740
- Rivinius T., Baade D., Hadrava P., Heida M., Klement R., 2020, *A&A*, 637, L3
- Rowan D. M., Thompson T. A., Jayasinghe T., Kochanek C. S., Stanek K. Z., 2024, arXiv e-prints, p. arXiv:2401.09531
- Ruitter A. J., 2019, *Proceedings of the International Astronomical Union*, 15, 1–15
- Sahu K. C., et al., 2022, *ApJ*, 933, 83
- Sana H., et al., 2012, *Science*, 337, 444
- Saracino S., et al., 2022, *MNRAS*, 511, 2914
- Sato Y., Nakasato N., Tanikawa A., Nomoto K., Maeda K., Hachisu I., 2015, *ApJ*, 807, 105
- Sato Y., Nakasato N., Tanikawa A., Nomoto K., Maeda K., Hachisu I., 2016, *ApJ*, 821, 67
- Schwab J., Quataert E., Bildsten L., 2015, *MNRAS*, 453, 1910
- Shahaf S., Hallakoun N., Mazeh T., Ben-Ami S., Rekh P., El-Badry K., Toonen S., 2023a, arXiv e-prints, p. arXiv:2309.15143
- Shahaf S., Bashi D., Mazeh T., Faigler S., Arenou F., El-Badry K., Rix H. W., 2023b, *MNRAS*, 518, 2991
- Shen K. J., et al., 2018, *ApJ*, 865, 15
- Shenar T., et al., 2022, *Nature Astronomy*, 6, 1085
- Shikauchi M., Kumamoto J., Tanikawa A., Fujii M. S., 2020, *PASJ*, 72, 45
- Shikauchi M., Tsuna D., Tanikawa A., Kawanaka N., 2023, *ApJ*, 953, 52
- Spitzer L., 1987, *Dynamical evolution of globular clusters*
- Tanikawa A., Nomoto K., Nakasato N., 2018, *ApJ*, 868, 90
- Tanikawa A., Nomoto K., Nakasato N., Maeda K., 2019, *ApJ*, 885, 103
- Tanikawa A., Hattori K., Kawanaka N., Kinugawa T., Shikauchi M., Tsuna D., 2023, *ApJ*, 946, 79
- Tanikawa A., Cary S., Shikauchi M., Wang L., Fujii M. S., 2024, *MNRAS*, 527, 4031
- Thompson T. A., et al., 2019, *Science*, 366, 637

- Toonen S., Nelemans G., Portegies Zwart S., 2012, *A&A*, 546, A70
- Wang L., Nitadori K., Makino J., 2020a, *MNRAS*, 493, 3398
- Wang L., Iwasawa M., Nitadori K., Makino J., 2020b, *MNRAS*, 497, 536
- Webbink R. F., 1984, *ApJ*, 277, 355
- Woosley S. E., Baron E., 1992, *ApJ*, 391, 228
- Woosley S. E., Taam R. E., Weaver T. A., 1986, *ApJ*, 301, 601
- Yamaguchi N., et al., 2024, *MNRAS*, 527, 11719
- Zenati Y., Perets H. B., Dessart L., Jacobson-Galán W. V., Toonen S., Rest A., 2023, *ApJ*, 944, 22
- Zheng L.-L., et al., 2023, *Science China Physics, Mechanics, and Astronomy*, 66, 129512
- van den Heuvel E. P. J., 2007, in di Salvo T., Israel G. L., Piersant L., Burderi L., Matt G., Tornambe A., Menna M. T., eds, *American Institute of Physics Conference Series Vol. 924, The Multicolored Landscape of Compact Objects and Their Explosive Origins*. pp 598–606 ([arXiv:0704.1215](https://arxiv.org/abs/0704.1215)), doi:10.1063/1.2774916
- van den Heuvel E. P. J., Tauris T. M., 2020, *Science*, 368, eaba3282

This paper was built using the Open Journal of Astrophysics \LaTeX template. The OJA is a journal which

provides fast and easy peer review for new papers in the **astro-ph** section of the arXiv, making the reviewing process simpler for authors and referees alike. Learn more at <http://astro.theoj.org>.